

Co-published by Institute of Fluid-Flow Machinery Polish Academy of Sciences

Committee on Thermodynamics and Combustion

Polish Academy of Sciences

Copyright@2025 by the Authors under licence CC BY 4.0

http://www.imp.gda.pl/archives-of-thermodynamics/



Numerical analysis of the effect of chemical reaction and heat source on MHD hyperbolic tangent fluid flow across a non-linear stretching sheet in a porous medium

Srinivas Reddy Kallem^a, Siva Reddy Sheri^{a*}, Alfunsa Prathiba^b, Gollapalli Shankar^c

Department of Mathematics, GSS, GITAM (Deemed to Be University), Hyderabad, Telangana-502329, India
 Department of Mathematics, CVR College of Engineering, Telanagana-501510, India
 Department of Mathematics, B V Raju Institute of Technology, Narsapur, Medak, Telanagana-502313, India
 *Corresponding author email: sreddy7@yahoo.co.in

Received: 10.09.2024; revised: 01.02.2025; accepted: 03.02.2025

Abstract

This study investigates the influence of chemical reactions, heat sources, and magnetohydrodynamic effects on the flow of hyperbolic tangent fluid over a nonlinear stretching sheet in a porous medium. Despite significant research on magnetohydrodynamic flows, the combined effects of magnetohydrodynamics, chemical reactions and heat on hyperbolic tangent fluid flow in porous media have not been fully explored, especially under varying electromagnetic conditions. This gap is critical in applications such as geothermal energy extraction, petroleum recovery, polymer processing and cooling systems for electronics. The governing equations for mass, momentum, energy and species transport are transformed into a dimensionless system using similarity transformations and solved numerically using the implicit finite difference method with MATLAB's "bvp4c" solver. Key parameters, including magnetic field strength, porosity, chemical reaction rate and heat source/sink are analysed for their effects on velocity, temperature and concentration profiles. Notably, varying magnetic field strengths significantly influence flow characteristics, offering insights into the behaviour of hyperbolic tangent fluid under different electromagnetic conditions. Results of this study show that magnetohydrodynamic interactions, chemical processes and thermal effects significantly affect the flow dynamics and heat transfer. Additionally, as the Darcy number increases and the permeability of the porous medium rises, so do the shear rates within the pores. This observation underscores the intricate relationship between the shear-thinning behaviour of heat transfer fluids and permeability, providing valuable insights for optimizing flow dynamics in porous media relevant to energy extraction and material processing applications.

Keywords: Chemical reaction; Tangent hyperbolic nanofluid; Heat source; Magnetohydrodynamic effects; Porous medium

Vol. 46(2025), No. 2, 57-67; doi: 10.24425/ather.2025.154906

Cite this manuscript as: Kallem, S.R., Sheri, S.R., Prathiba, A., & Shankar, G. (2025). Numerical analysis of the effect of chemical reaction and heat source on MHD hyperbolic tangent fluid flow across a non-linear stretching sheet in a porous medium. *Archives of Thermodynamics*, 46(2), 57–67.

1. Introduction

The mathematical modelling of heat and mass transfer in nanofluid (NF) flow has sparked widespread attention due to its broad ramifications in a variety of disciplines of applied research and advanced technology. It has several uses in geosciences, the petroleum sector, biotechnology, and biomedicine. As a result, various researchers have studied magnetohydrodynamic (MHD) convection mass and heat transfer in NF flow

problems. Shankar Goud et al. [1] numerically analysed the effects of the Eckert and Prandtl numbers on MHD natural convection of an electrically conducting, incompressible viscous fluid flowing through a perpendicular microchannel. The study considered conduction in non-conducting walls and temperature/velocity slip. The coupled momentum and induction equations, accounting for the induced magnetic field, were transformed into nonlinear ordinary differential equations (ODEs) using similarity variables and solved numerically using MAT-

Nomenclature

C – concentration profile, mol

 C_f – skin friction coefficient

 C_w – concentration of fluid at the wall, mol

 C_{∞} – ambient concentration of fluid, mol

 D_B – Brownian diffusion coefficient, m²/s

 D_T – thermophoresis diffusion coefficient, m²/s

Ec - Eckert number

 $f'(\eta)$ – velocity profile

g – gravitational acceleration, m²/s

 $g(\eta)$ – dimensionless concentration profile

M − magnetic parameter

n – fluid shear thinning behaviour

Nbt- thermophoretic parameter

Nc - Brownian motion parameter

Nux-local Nusselt number

Pr - Prandtl number

Q – heat source parameter

R – radiation parameter

Rc – chemical reaction parameter

Rex-local Reynolds number

Sc - Schmidt number

Sh_x – local Sherwood number

T – fluid temperature, K

 T_w – surface temperature, K

 T_{∞} – ambient temperature, K

u, v – velocity components, m/s

 u_w – velocity at the wall, m/s

We - Weissenberg number

x, y – Cartesian coordinates, m

Greek symbols

 α – thermal diffusivity, m²/s

 Γ – positive time constant

 η – dimensionless similarity variable

 $\theta(\eta)$ – temperature profile

 μ – dynamic viscosity, Pa·s

v – kinematic viscosity, m²/s

 ρ – density, kg/m³

 σ – electrical conductivity, S/m

Subscripts and Superscripts

 ∞ - condition at the free stream

w - condition at the surface

Abbreviations and Acronyms

ANN – artificial neural networks

HTF - hyperbolic tangent fluid

MHD- magnetohydrodynamic

NF - nanofluid

NSP - nonlinear stretching plate

NSS - nonlinear stretching sheet

LAB. Graphical results showed that increasing the Hartmann and magnetic Prandtl numbers significantly reduces the volume flow rate. Al Oweidi et al. [2] investigated entropy generation in MHD mixed convection of a Casson nanofluid with Arrhenius activation energy over a nonlinearly stretching sheet and solved it numerically with MATLAB's bvp4c solver. The study showed that increasing the slip parameter increases temperature and decreases entropy generation, while the Brinkman number and concentration gradient have opposing effects on entropy. The Eckert number's influence on temperature is amplified by the presence of nanoparticles. The results were validated by comparison with previous studies. Jamshed et al. [3] explored the effect of electromagnetic radiation and convective slippery circumstances on second-grade nanofluids with permeability. Pal [4] investigated heat and mass transfer in the two-dimensional stagnation-point flow of an incompressible viscous fluid over a stretching vertical sheet, considering the effects of buoyancy force and thermal radiation. Their results, presented in tabular form, demonstrated that thermal radiation leads to an increase in the skin friction coefficient, local Nusselt number and Sherwood number. Asogwa et al. [5] studied Cu-H₂O nanofluids flow past the upright Riga plate, comparing isothermal and ramped wall temperature scenarios. Kandasamy et al. [6] analysed the impact of temperature-dependent fluid viscosity, chemical reactions and thermophoresis on MHD free convective heat and mass transfer in the presence of heat generation/absorption, considering flow over a porous stretching sheet. Dharmaiah et al. [7] numerically analysed heat and mass transfer with viscous dissipation, Joule dissipation and activation energy. Building upon this work, Goud et al. [8] extended the investigation to explore the role of Joule heating and activation energy on MHD

heat and mass transfer flow in the presence of thermal radiation. Elbashbeshy and Bazid [9] investigated the thermal transport characteristics of NF flow across an unstable stretched sheet, considering the wobbliness metric and "Prandtl number" (Pr). Raptis [10] explored radiant heat transfer and spontaneous convection in porous media. Cortell [11] studied heat transfer in the flow of a viscous fluid over a nonlinear stretching plate (NSP). Xuan and Li [12] conducted a theoretical investigation of the thermal conductivity of nanofluids, accounting for the volume fraction, shape and size of nanoparticles.

The HTF model is a popular variant of the classic "non-Newtonian model" used in chemical engineering because it is computationally efficient, durable and practical. In contrast to empirical connections, this rheological model is based on the liquid kinetic theory, making it a more basic and dependable alternative. Although no one model can completely represent the complicated features of non-Newtonian fluids, the hyperbolic tangent model is an effective tool for understanding their behaviour. Researchers have used this model to examine several elements of non-Newtonian fluid dynamics. For instance, the MHD flow of HTF around a stretched cylinder using the Keller box method was investigated by Malik et al. [13]. Naseer et al. [14] studied the steady boundary layer flow and heat transfer of a tangential hyperbolic fluid flow in the presence of a vertically stretched cylinder. Hayat et. al. [15] investigated the chemically reactive flow of HTF with heat radiation and dual stratification in a porous medium. Nadeem and Akram [16] explored an extensive study on the peristaltic transport of HTF in an asymmetric channel. Reddy et al. [17] in their investigations on MHD hyperbolic tangent fluid flow across a non-linear stretching sheet in a porous medium, focused instead on boundary layer flow and thermophysical properties by implementing the Keller box method. Additional relevant studies involving stretching sheets can be found in the literature, Upadhya et al. [18] and Nadeem and Akram [19].

Convective flow accompanied by concurrent mass and heat transport with chemical reactions is a ubiquitous phenomenon in various applications. Notably, such methods are widespread in the chemical field, power generation and cooling sectors, dyeing, chemical vapour plating on surfaces, nuclear reactor cooling and fossil fuel sectors. Chemical reactions are categorized as either consistent or diverse processes, depending on whether they manifest at a junction or as a singular-phase reaction within a volume. A uniform-phase reaction occurs evenly throughout a given medium, whereas a heterogeneous reaction is restricted to a particular zone or phase surface. The rate of reaction is primarily concentration-dependent, and for first-order reactions, it varies linearly with the concentration. For instance, the creation of smog is a first-order chemical reaction that occurs uniformly throughout the phase, resulting from the discharge of NO₂ from vehicles and chimneys, which exhibits similar behaviour to unburned hydrocarbons skyborne with sunlight influence, to produce "acetyl peroxyl nitrate" C₂H₃NO₅, forming a photochemical smog envelope. Sheikh et al. [20] investigated in their study an MHD flow and focused on the effect of chemically reactive species over a stretching sheet, considering thermal radiation and partial slip. Nasir et al. [21] considered the 3D radiative flow of a tangent hyperbolic fluid across a porous stretched sheet using artificial neural networks (ANN) backpropagation and Bayesian regularization. The Cattaneo-Christov flow model, heat radiation, chemical processes and ion slip effects were all included in their study, which used MATLAB's BVP4C solver to train ANN. ANN obtained a great accuracy (R2 = 1, MSE \approx 10-11), reducing the fluid velocity with increased porosity and magnetic parameters, while increasing the thermal profile. Their discoveries have major implications for modern cooling and heating technology. Gaffar et al. [22] explored thermal convection flow of magnetized tangent hyperbolic fluid around a spinning cone in a porous medium using the Brinkman-Darcy-Forchheimer model. The Keller Box approach was used to investigate the fluctuations in velocity, temperature, skin friction and Nusselt number with respect to critical factors. The results revealed that raising the Weissenberg number, Forchheimer number and radiative flux lowered velocities while increasing temperature, whereas higher Darcy numbers increased the velocity near the cone but decreased the temperature.

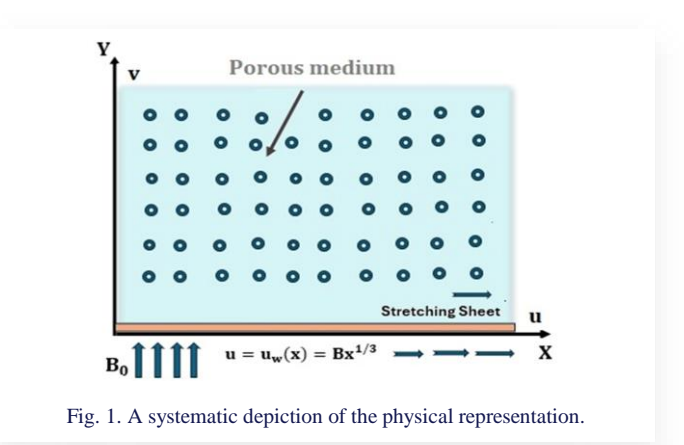
Further in line with those findings, the study of Shehzad et al. [23] also observes a more rapid decrease in the concentration profile compared to the fluid velocity with an increase in the suction parameter. These findings provide valuable insights into the behaviour of Casson fluids under the combined influence of MHD, mass transfer and chemical reactions.

This study aims to explore the flow dynamics and heat transfer characteristics of a two-dimensional magnetohydrodynamic nanofluid incorporating the hyperbolic tangent velocity model over a nonlinearly stretching sheet. As an extension of the work of Amjad et al. [24] and Ahmed et al. [25], the analysis focuses

on understanding the interplay between nonlinear stretching effects, magnetic field influence and nanofluid properties to provide deeper insights into the behaviour of such complex fluid systems. The partial differential equations (PDEs) that govern the flow with the corresponding boundary conditions are transformed into highly nonlinear ODEs using a similarity transformation. The resulting ODEs were numerically solved using the bvp4c solver. The effects of varying key metrics on the velocity, temperature and concentration profiles were examined through graphs.

2. Problem description

In this model (Fig. 1), we consider the ongoing movement of HTF with a fixed density through a nonlinear stretching sheet (NSS). The stretching sheet speed in the *x*-direction is defined as $u = u_w(x) = Bx^{1/3}$, whilst that in the *y*-direction is orthogonal. We postulated a two-dimensional incompressible layer of boundary fluid and investigated the impact of magnetohydrodynamics (MHD). The *y*-axis receives a tunable transverse magnetic field $B = B_0 x^{-1/3}$ (where B_0 is the magnetic flux). T_∞ , T_w , C_w and C_∞ denote the ambient temperature, wall temperature, surface concentration and ambient concentration of the fluid, respectively.



The theoretical equations for the numerical simulation of the hyperbolic tangent fluid (HTF) flow together with the postulated boundary circumstances are shown below (Amjad et al. [24]):

$$\frac{\partial u}{\partial x} + \frac{\partial v}{\partial y} = 0,\tag{1}$$

$$u \frac{\partial u}{\partial x} + v \frac{\partial u}{\partial y} = \vartheta \left((1 - n) + \sqrt{2} n \Gamma \frac{\partial u}{\partial y} \right) \frac{\partial^2 u}{\partial y^2} - \frac{\sigma B_0^2(x)}{\rho} u + \frac{\vartheta}{\kappa} u + g \beta^* (T - T_\infty) + g \beta_c (C - C_\infty),$$
 (2)

$$u\frac{\partial T}{\partial x} + v\frac{\partial T}{\partial y} = \alpha\frac{\partial^2 T}{\partial y^2} + \frac{\rho_p\,c_p}{\rho\,c} \left[D_B \frac{\partial C}{\partial y} \frac{\partial T}{\partial y} + \frac{D_T}{T_\infty} \left(\frac{\partial T}{\partial y} \right)^2 \right] + \frac{\mu}{\rho c} \left(\frac{\partial u}{\partial y} \right)^2 +$$

$$+\alpha \frac{\partial q_r}{\partial y} + \frac{Q_0}{\alpha c} (T - T_{\infty}),$$
 (3)

$$u\frac{\partial c}{\partial x} + v\frac{\partial c}{\partial y} = \frac{D_T}{T_{\infty}}\frac{\partial^2 T}{\partial y^2} + D_B \frac{\partial^2 C}{\partial y^2} - R_0(C - C_{\infty}). \tag{4}$$

The associated boundary conditions are Ahmed et al. [25]:

Kallem S.R., Sheri S.R., Prathiba A., Shankar G.

at
$$y = 0$$
,
$$\begin{cases} u = u_w(x) = Bx^{1/3} \\ v = 0 \\ T = T_w \\ C = C_w \end{cases}$$
 as $y \to \infty$,
$$\begin{cases} u \to 0 \\ T \to 0 \\ C \to 0 \end{cases}$$
 (5)

Here, n, σ^* , K, μ , ϑ , Γ , B_0 , ρ , c, Q_0 , R_0 , q_r , α , β_c , β^* , ρ_p and c_p represent shear-thinning behaviour of the fluid, Stefan-Bolzmann constant, porous medium permeability, dynamic viscosity, kinematic viscosity, time constant, magnetic field, density, specific heat, heat source coefficient, chemical reaction coefficient, radiative heat flux, thermal diffusivity, concentration expansion coefficient, thermal expansion coefficient, density and specific heat of particle, respectively. Using the following similarity transformations (Amjad et al. [24])

$$\begin{cases} u = \frac{\partial \Psi}{\partial y} = Bx^{1/3} f'(\eta) \\ v = -\frac{\partial \Psi}{\partial x} = -\frac{\sqrt{\vartheta B}}{3x^{1/3}} [2f(\eta) - \eta f'(\eta)] \\ \eta = \frac{y}{x^{1/3}} \sqrt{\frac{B}{\vartheta}}, g = \frac{C - C_{\infty}}{C_{w} - C_{\infty}}, \theta = \frac{T - T_{\infty}}{T_{w} - T_{\infty}} \\ q_{r} = \frac{16 \sigma^{*} T_{\infty}^{3}}{3kk^{*}} \frac{\partial T}{\partial y} \\ K_{0} = K x^{-2/3} \end{cases}$$
 (6)

in Eqs. (2), (3), (4) and (5) leads to the dimensionless form of equations as:

$$[(1-n) + n \operatorname{We} f''] * f''' - \frac{f'^2}{3} - M \cdot f' + \frac{2}{3} f \cdot f'' +$$

$$-\operatorname{Da} \cdot f' + \operatorname{Gr} \cdot \theta + \operatorname{Gc} g = 0, \tag{7}$$

$$\frac{2}{3} \operatorname{Pr} \theta' f + [1 + \frac{4R}{3}] \theta'' + \frac{Nc}{\operatorname{Le}} g' \theta' + \frac{Nc}{\operatorname{Le} Nbt} \theta'^2 +$$

$$+\operatorname{Pr} Q \theta + \operatorname{Pr} \operatorname{Ec} f^{\prime\prime 2} = 0, \tag{8}$$

$$g' + \frac{2}{3} \operatorname{Sc} g' f + \frac{1}{Nbt} \theta'' - \operatorname{Sc} R_c g = 0.$$
 (9)

Then dimensionless BC (boundary conditions) are:

$$at \eta = 0, \begin{cases} f' = 1 \\ f = 0 \\ \theta = 1 \\ g = 1 \end{cases} \quad as \eta \to \infty, \begin{cases} f' \to 0 \\ \theta \to 0 \\ g \to 0 \end{cases}$$
 (10)

The dimensionless parameters used in these equations are:

$$\begin{cases} We = \sqrt{\frac{2B^{3}}{\vartheta}}, M = \frac{\sigma B_{0}^{2}}{B \rho} x^{\frac{2}{3}}, Gr = \frac{g \beta^{*} (T_{W} - T_{\infty})}{B^{2} x^{-\frac{1}{3}}}, Le = \frac{\alpha}{D_{B}} \\ Gc = \frac{g \beta_{c} (C_{W} - C_{\infty})}{B^{2} x^{-\frac{1}{3}}}, R = \frac{4 \sigma^{*} T_{\infty}^{3}}{k k^{*}}, Pr = \frac{\vartheta}{\alpha} = \frac{Sc}{Le}, Sc = \frac{\vartheta}{D_{B}} \\ Nc = \frac{\rho_{p} c_{p}}{\rho c} (C_{W} - C_{\infty}), Nbt = \frac{D_{B} T_{\infty} (C_{W} - C_{\infty})}{D_{T} (T_{W} - T_{\infty})} \\ Q = \frac{Q_{0} x^{2/3}}{B \rho c}, Ec = \frac{u_{W}^{2}}{c (T_{W} - T_{\infty})}, Da = \frac{\vartheta}{B K_{0}}, R_{c} = \frac{R_{0} x}{u_{W}} \end{cases}$$
(11)

Here, R_c , R, Le, Ec, Gr, Gc, k, k^* and Ψ represent chemical reaction factor, radiation factor, Lewis number, Eckert number, thermal, solutal Grashof numbers, thermal expansion, mean absorption coefficient and stream function.

The skin friction coefficient C_f , Nu_x (Nusselt number), Sh_x (Sherwood number) are given below:

$$\begin{cases}
C_f = \frac{\tau_w}{\rho u_w^2}, \quad \tau_w = \mu \frac{\partial u}{\partial y} \Big|_{y=0} \\
\operatorname{Nu}_x = \frac{xq_w}{k (T_w - T_\infty)}, \quad q_w = -k \frac{\partial T}{\partial y} \Big|_{y=0} \\
\operatorname{Sh}_x = \frac{xq_s}{D_B (C_w - C_\infty)}, \quad q_s = -D_B \frac{\partial C}{\partial y} \Big|_{y=0}
\end{cases}.$$
(12)

Here, τ_w , q_w and q_s represent shear stress, surface heat flux and mass flux.

The above equations after applying the similarity transformation and simplification are given as:

$$\begin{cases}
C_f \operatorname{Re}_x = \left[(1 - n) + \frac{n}{2} \operatorname{We} f''(0) \right] f''(0) \\
\frac{\operatorname{Nu}_x}{\operatorname{Re}_x} = -\theta'(0) \\
\frac{\operatorname{Sh}_x}{\operatorname{Re}_x} = -g'(0), \\
\operatorname{where:} \operatorname{Re}_x = \frac{u_w^2}{\sqrt{B^3 \vartheta}} = x^{2/3} \sqrt{B/\vartheta}
\end{cases} . \tag{13}$$

3. Mathematical procedure

The system of coupled nonlinear ordinary differential equations (ODE) as derived in Eqs. (7)–(9), subject to the boundary conditions (BC) defined in Eq. (10), were solved numerically using MATLAB's byp4c solver. This solver employs a finite difference method based on the 3-stage Lobatto IIIa formula (LeVeque [26]). To utilize byp4c, Eqs. (7)–(9), are first transformed into a set of coupled first-order ODEs, enabling the problem to be formulated as a boundary value problem. A finite value of $\eta \to \infty$ was assumed for $\eta = 40$ – the far-field boundary condition. The bvp4c solver requires three inputs: the ODE function (odes), boundary condition residual function (bcs) and an initial guess for the solution and mesh (solinit). Numerical solutions were then obtained for various parameters of the governing equations: the power-law index n, Weissenberg number We, Prandtl number Pr, magnetic parameter M, Brownian motion parameter Nbt, thermophoresis parameter Nc and Darcy number Da. The ordinary differential Eqs. (7)–(9), as well as the boundary conditions in Eq. (10), are transformed into a first-order equation system by introducing new variables. The following transformation is applied:

$$y_{1} = f(\eta), \qquad y_{1}' = y_{2},$$

$$y_{2} = f'(\eta), \qquad y_{2}' = y_{3},$$

$$y_{3} = f''(\eta), \qquad y_{3}' = \frac{\frac{(y_{2})^{2}}{3} + M y_{2} - \frac{2}{3} y_{1} y_{3} + Da y_{2} - Gr y_{4} - Gc y_{6}}{(1-n) + n \operatorname{We} y_{3}},$$

$$y_{4} = \theta(\eta), \qquad y_{4}' = y_{5},$$

$$y_{5} = \theta'(\eta),$$

$$y_{5}' = \frac{-\frac{2}{3}\operatorname{Pr} y_{1} y_{5} - \frac{Nc}{\operatorname{Le}} y_{5} y_{7} - \frac{Nc}{\operatorname{Le} Nb_{t}} (y_{5})^{2} - \operatorname{Pr} Q y_{4} - \operatorname{Pr} \operatorname{Ec} (y_{3})^{2}}{\left[1 + \frac{4R}{3}\right]},$$

$$y_{6} = g(\eta), \qquad y_{6}' = y_{7},$$

$$y_{7} = g'(\eta), \qquad y_{7}' = -\frac{2}{3} \operatorname{Sc} y_{1} y_{7} - \frac{y_{5}'}{\operatorname{Nb_{t}}} + S_{c} R_{c} y_{6},$$

subjected to:

$$y_1(0) = a$$
, $y_2(0) = b$, $y_3(0) = b_1$, $y_4(0) = b$, $y_5(0) = b_2$, $y_6(0) = b$, $y_7(0) = b_3$, $y_2(\infty) = a$, $y_4(\infty) = a$, $y_6(\infty) = a$,

where: a = 0, b = 1.

4. Results and discussion

This segment delivers graphs and tables showing how different physical parameters affect dimensionless speed, temperature and concentration. Table 1 shows the effect of the parameters n, M and the Weissenberg number (We) on the skin friction coefficient $\operatorname{Re}_x C_f$, Ahmed et al. [25]. Skin friction rises with both n and M, but decreases with the Weissenberg number for $\operatorname{Da=Gr=Gc=0}$. Table 2 shows how n, We, M, Pr , Le , Nc , Nbt and Sc affect $-\theta'(0)$ and -g'(0), $R=\operatorname{Ec=0}$. It is seen that $-\theta'(0)$ rises with Pr , Le , Nbt and Sc , whereas it decreases with n, We , M and Nc . Similarly, the Sherwood number -g'(0) grows with Nc , Nbt

and Sc, but decreases with n, We, M, Pr and Le. Table 3 shows the numerical findings for the Nusselt number $-\theta'(0)$ for various We and Pr values. Tables 1–3 show that our findings are congruent with those of Ahmed et al. [25]. The influence of the metrics Rc, R, Q, M and Da on the velocity profile can be observed from Figs. 2–6.

Table 1. Effect of n, We, M on skin friction coefficient Re_xC_f with Da = Gr = Gc = 0.

n	We	M	Re_xC_f [25]	Re_xC_f
0.1	0.5	0.5	0.932163	0.943621
0.2			1.016640	1.16139
0.3			1.096308	1.124345
0.3	0.1		0.808646	0.823561
	0.2		0.800995	0.829672
	0.3		0.793042	0.793240
		0.1	0.600077	0.600100
		0.2	0.648990	0.648899
		0.3	0.694237	0.694221

Table 2. Effect of n, We, M, Pr, Le, Nc, Nbt, Sc on $-\theta'(0)$, -g'(0) for R=Ec=0.

n	We	M	Pr	Le	Nc	Nbt	Sc	− <i>Θ'</i> (0) [25]	-g'(0) [25]	− <i>Θ'</i> (0)	<i>−g</i> ′(0)
0.1								0.209793	0.627703	0.209534	0.628793
0.2								0.200519	0.610165	0.202132	0.612128
0.3								0.189534	0.587607	0.188235	0.589021
0.3	0.1							0.191385	0.597856	0.198037	0.598213
	0.2							0.190240	0.595289	0.196452	0.596253
	0.3							0.189048	0.592585	0.189274	0.593630
		0.1						0.218816	0.645472	0.219125	0.646203
		0.2						0.209244	0.629025	0.208269	0.629294
		0.3						0.200779	0.613862	0.201943	0.614204
			0.1					0.063744	0.635271	0.064247	0.636367
			0.2					0.091398	0.622241	0.092156	0.623464
			0.3					0.122145	0.609816	0.123206	0.609048
			0.5	0.1				0.001045	0.651501	0.002105	0.652479
				0.2				0.016199	0.646421	0.017345	0.646532
				0.3				0.039595	0.649343	0.038649	0.649689
					0.1			0.212768	0.576634	0.213185	0.577839
					0.2			0.205897	0.579276	0.206064	0.571094
					0.3			0.199232	0.581832	0.199568	0.582120
						0.1		0.104454	0.046621	0.156023	0.047864
						0.2		0.139576	0.224951	0.138673	0.225207
						0.3		0.154879	0.330159	0.155783	0.331075
							0.1	0.206840	-0.005330	0.207356	-0.006552
							0.2	0.204218	0.026183	0.205720	0.025294
							0.3	0.201683	0.062341	0.202075	0.063360

Table 3. Effect of We, Pr on -g'(0).

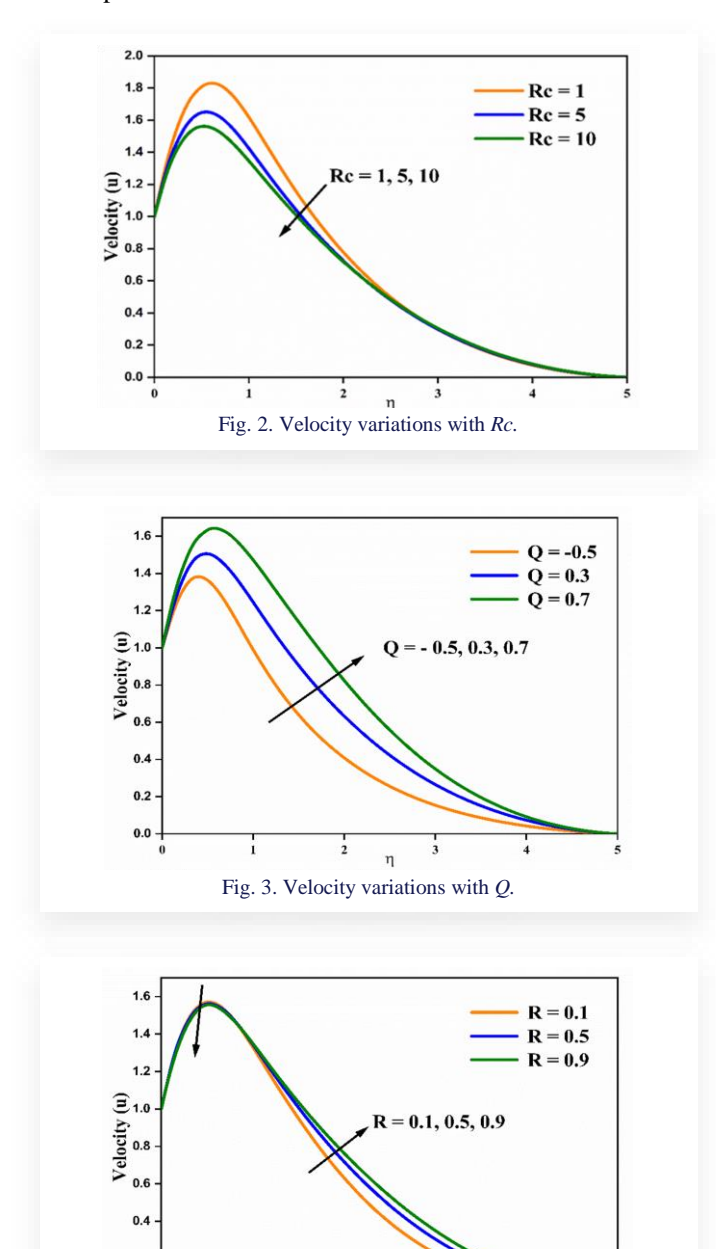
We	Pr	-g'(0) [25]	<i>−g</i> ′(0)
0.0	0.5	0.319	0.322
0.2		0.318	0.321
0.4		0.317	0.320
	0.2	0.231	0.234
	0.6	0.348	0.351
	1.2	0.521	0.524

In Fig. 2, the increased chemical reaction rate leads to a decreased fluid velocity. A possible explanation for this could be

that higher reaction rates lead to increased consumption of reactants, which might result in a less dense and slower-moving fluid. Beyond $\eta \sim 2.5$, the velocity likely enters a regime where the system reaches an equilibrium or a steady state. Here, the effects of Rc diminish, due to the velocity profile flattening out as it approaches a far-field condition, the influence of dominant forces, inertial forces overtaking the variations induced by Rc.

In Figs. 3 and 4, increased heat source/sink and radiation values lead to the increased fluid velocity. For $\eta < 1$, the flow is likely dominated by viscous forces in the boundary layer or near-wall area. Radiation effects are weaker here, leaving the velocity profile essentially unaltered. For $\eta > 1$, radiation has

a greater impact on the flow field due to the increased temperature, reduced viscosity from shear-thinning, and enhanced thermal expansion effects.



In Fig. 5, the increased magnetic field strength (M) leads to the decreased fluid velocity. This is consistent with the principles of MHD, where the magnetic field exerts a drag force on the conducting fluid, opposing its motion. The reduced Lorentz force affects as the flow passes away $(\eta > 3)$ from the border zone, the magnetic field impact lessens and the velocity becomes insensitive to M.

Fig. 4. Velocity variations with R.

Tangential hyperbolic fluids often exhibit shear-thinning behaviour, meaning their viscosity decreases with increasing shear rate. As Da increases, the permeability of the porous medium increases, potentially leading to higher shear rates within the pores (Fig. 6). This increased shear rate could cause a significant decrease in the fluid viscosity, counteracting the increased permeability, and result in a net decrease in velocity. With uniform flow through porous medium beyond a certain distance ($\eta > 3$), the flow reaches a domain where the influence of the porous medium resistance (connected to Da) is no longer substantial, and the velocity profile stabilizes.

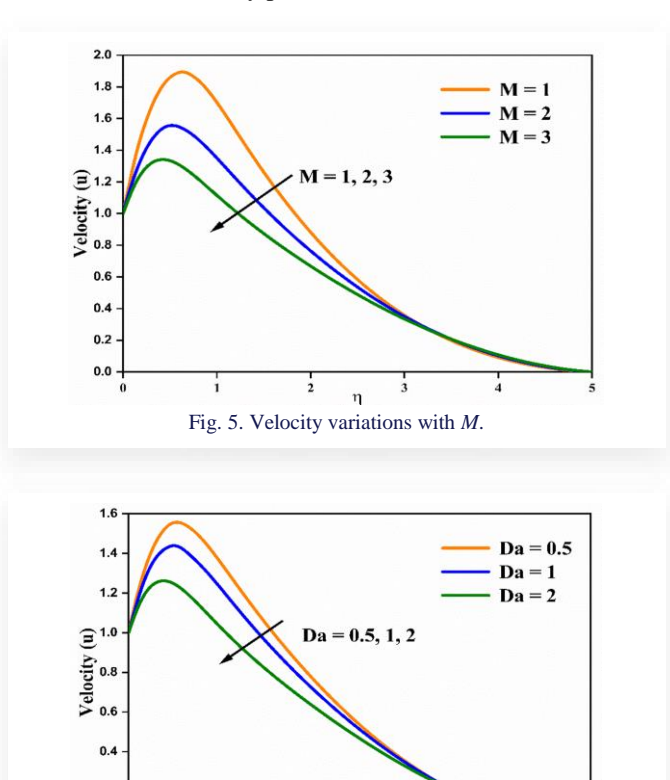
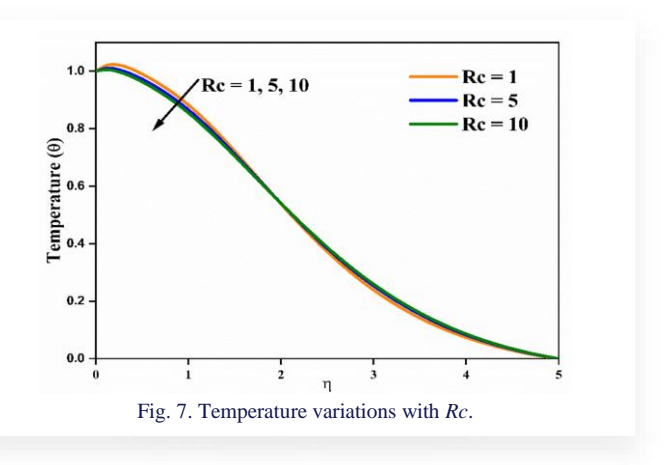


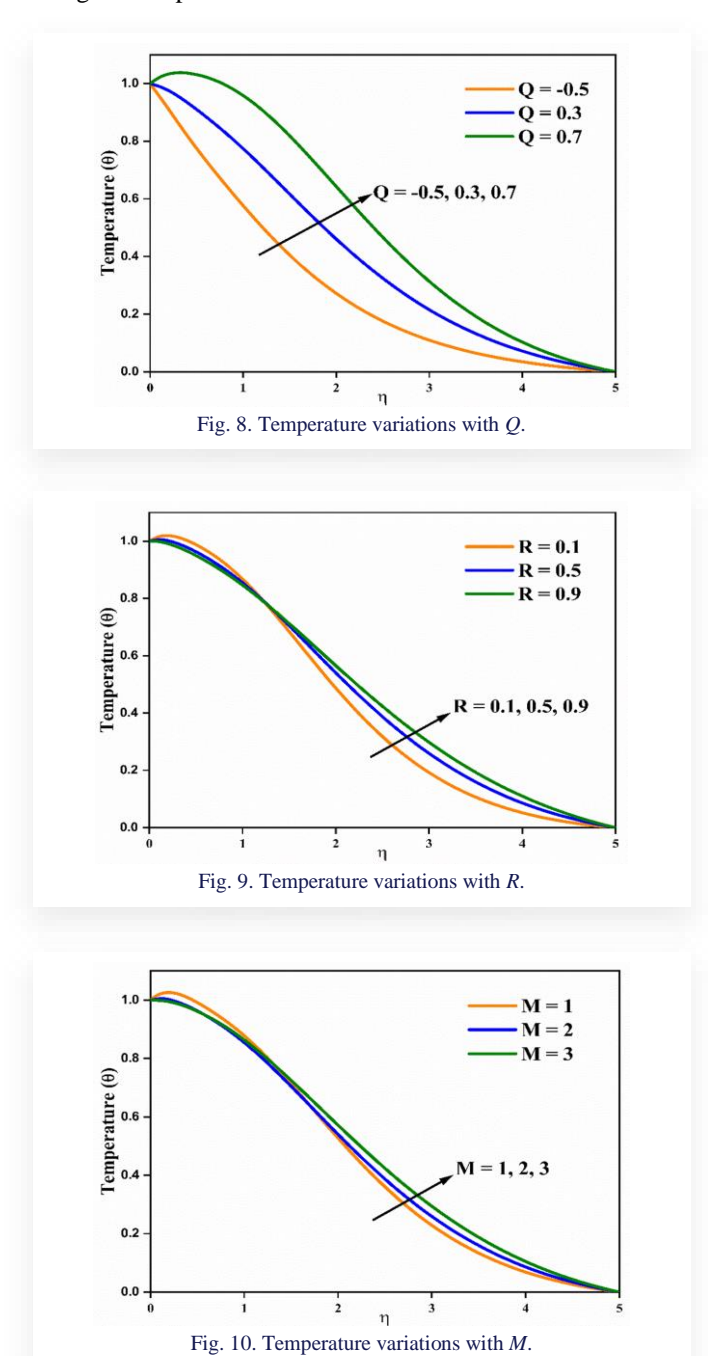
Figure 7 explores the temperature profile for varying values of the chemical reaction parameter Rc. The observed behaviour suggests a transition in the nature of heat transfer around $\eta=2$. In this model, the influence of chemical reactions or other complex phenomena is represented by a term, $S(\eta) = Sc \cdot Rc \cdot g(\eta)$ in the energy equation. For $\eta < 2$, $S(\eta)$ acts as a heat sink (endothermic), leading to a decrease in temperature with increasing Rc. Conversely, for $\eta > 2$, $S(\eta)$ acts as a heat source (exothermic), resulting in the expected increase in temperature with increasing Rc.

Fig. 6. Velocity variations with Da.

0.0

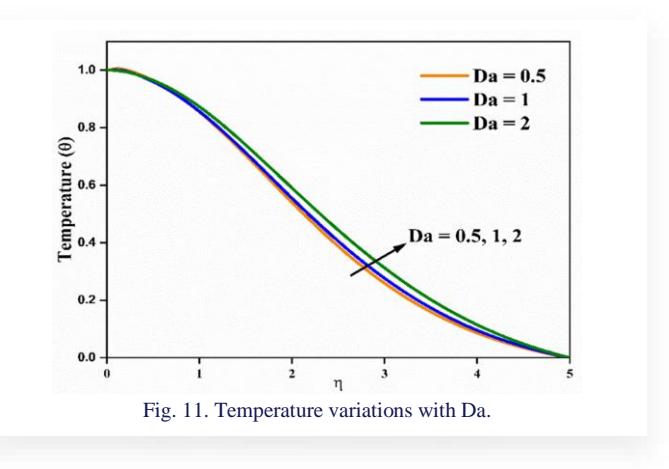


In Figs. 8 to 11, increased heat source, radiation, magnetic field and Da values lead to the increased fluid temperature. Heat source: adding heat to a system naturally increases its temperature. Magnetic field: a magnetic field can induce currents in a conductive fluid, leading to resistive heating. Darcy number: the Darcy number is related to fluid flow through porous media. A higher Da generally indicates greater flow, which can enhance heat transfer and increase the temperature. Radiation: increased radiation will lead to greater absorption of radiant energy, thus lifting the temperature.



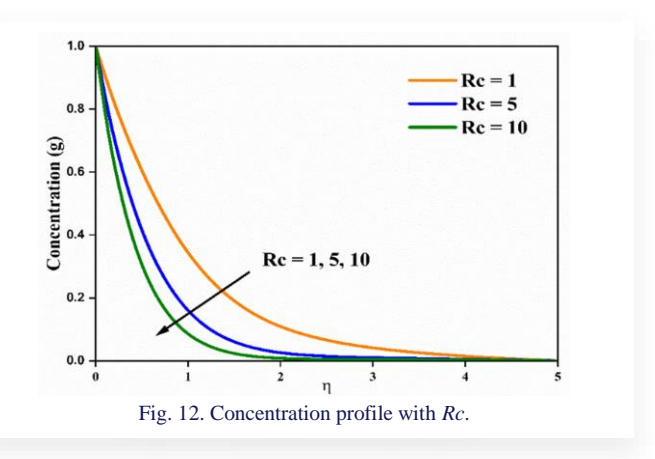
In Fig. 9, at smaller η values (η < 1.3), heat conduction is a more dominant mode of heat transfer. The influence of radiation is less pronounced in this region and other factors like the stretching surface or fluid properties cause a decrease in temperature despite the increase in R. Around η = 1.3, there is a transi-

tion region where the balance between conduction and radiation shifts. The increasing radiation might start to have a more significant effect, counteracting the factors that were causing the temperature to decrease at smaller η values. For larger η values ($\eta > 1.3$), radiation likely becomes the dominant mode of heat transfer. The increase in R directly leads to an increase in temperature in this region.



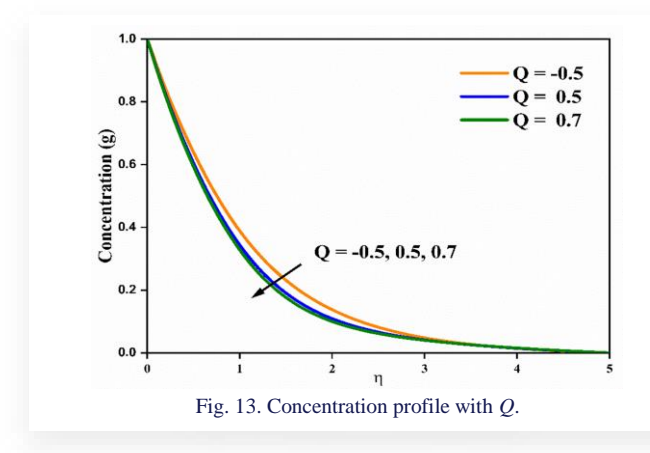
Figs. 10 and Fig. 11 explore the temperature profiles for varying values of the magnetic parameter (M) and Darcy number (Da). A distinct split behaviour is observed, for $\eta < 1.5$ approximately, increasing M leads to a decrease in temperature, while the opposite trend is observed for $\eta > 1.5$. This suggests a competition between several physical effects. Increasing M strengthens the Lorentz force, which can suppress convective heat transfer in certain regions while enhancing it in others. Similarly, increasing Da suppress the temperature field for $\eta < 1$; for $\eta > 1$, having opposing effects on the temperature. The combined influence of M and Da, coupled with the effects of buoyancy (represented by Gr), the boundary conditions at the stretching sheet and the non-linear nature of the governing equations lead to the complex temperature distribution observed. It was found that the influence of other parameters, such as Pr and Le is crucial.

The chemical reaction parameter Rc influences the fluid dynamics because the chemical reaction affects momentum and energy transfer due to changes in concentration or thermal gradients. This is where the velocity is sensitive to Rc and a decrease in concentration profile is observed due to the combined effects of the chemical reaction and fluid resistance as observed in Fig. 12.

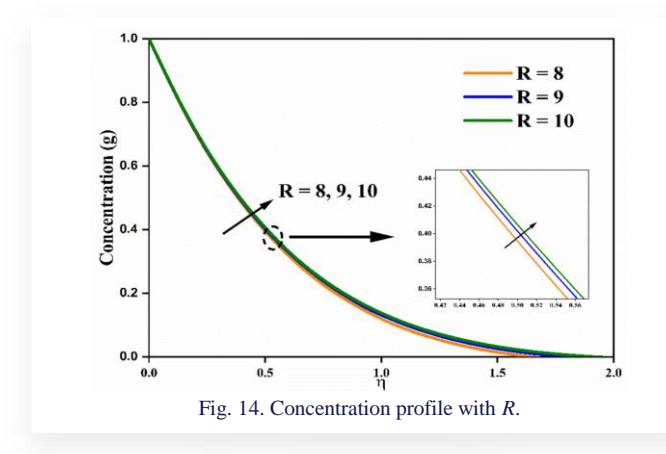


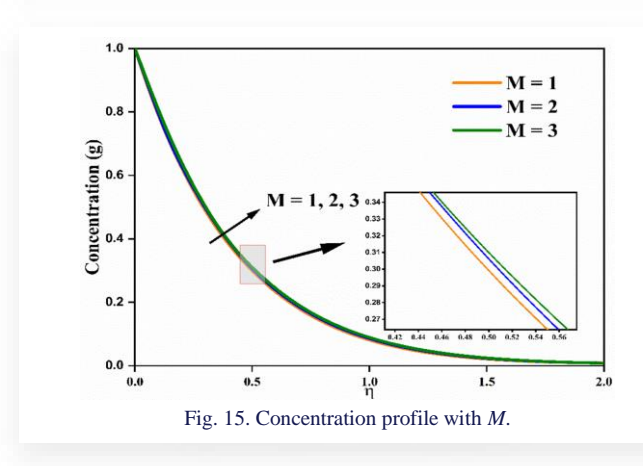
Since velocity, temperature and concentration profiles are coupled in the boundary layer, any effect of Rc on the fluid flow is localized near the surface (small η). At large η , the influence of chemical reactions vanishes, leading to identical profiles regardless of the value of Rc.

As shown in Fig. 13, the effect of heat on concentration depends on the heat source parameter. Exothermic reactions tend to shift towards reactants at higher temperatures, potentially leading to increased reactant concentration. Endothermic reactions shift towards products at higher temperatures, potentially leading to a decreased reactant concentration.

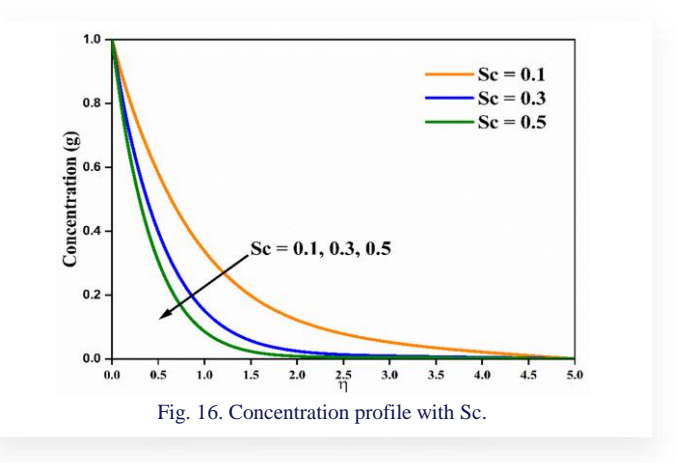


From Figs. 14 and 15 we observe that increased radiation and magnetic parameter values lead to the rise in the concentration profiles. There is a poor coupling between R and M and other system parameters, resulting in little visible variations.

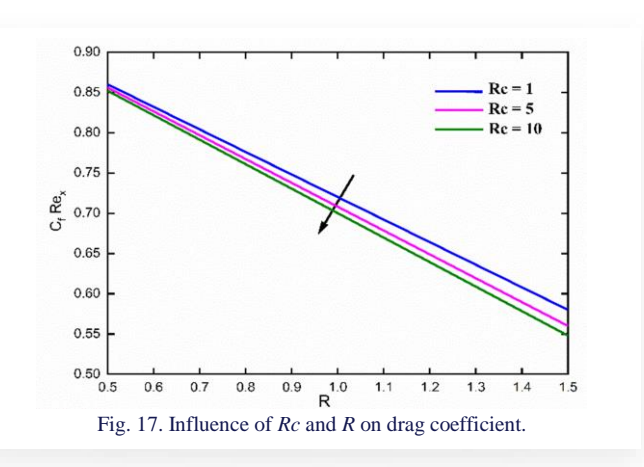


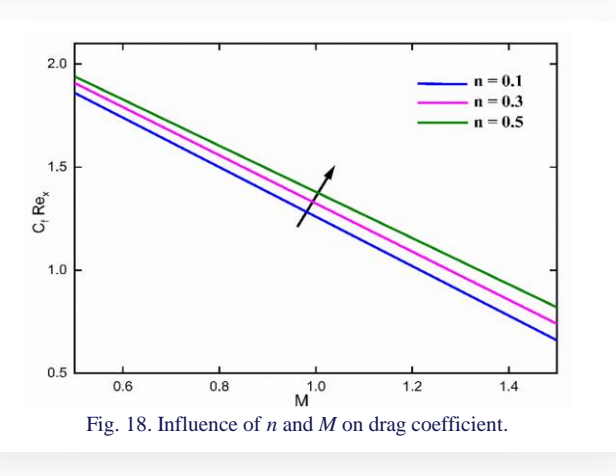


The Schmidt number describes the relative effectiveness of momentum diffusion (viscosity) compared to mass diffusion. A higher Sc means that momentum diffusion dominates, which can lead to thinner boundary layers and potentially higher concentration gradients near a surface, but lower concentrations overall (Fig. 16).



The impact of the different metrics on the drag coefficient and Nu can be visualized from Figs. 17 to 23. The skin friction coefficient exhibits a complex interplay with the magnetic field, fluid elasticity, flow behaviour and slip parameter. While increasing the magnetic field strength initially enhances skin friction, this effect reverses beyond a certain threshold.





Similarly, the coefficient initially rises with the increasing power-law index, indicating a complex relationship between flow behaviour and friction. Increased fluid elasticity, represented by the Weissenberg number, generally reduces skin friction, following a downward parabolic trend.

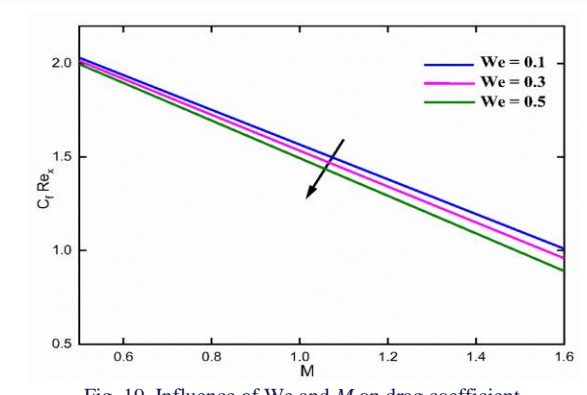


Fig. 19. Influence of We and M on drag coefficient.

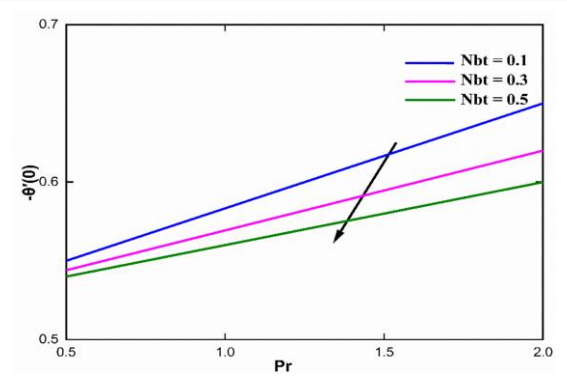


Fig. 20. Influence of Nbt and Pr on local Nusselt number.

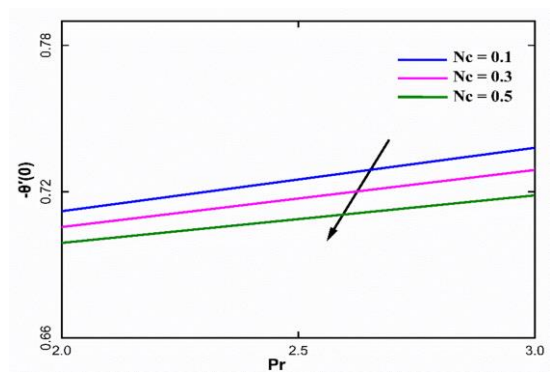


Fig. 21. Influence of Nc and Pr on local Nusselt number.

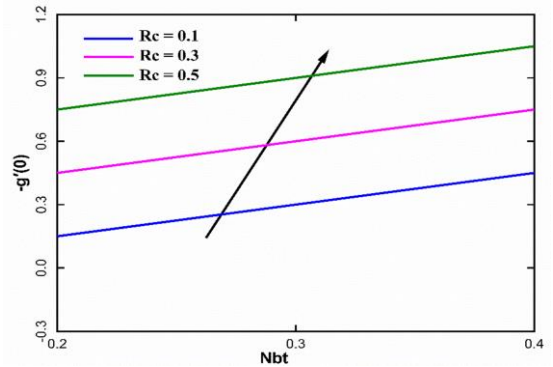
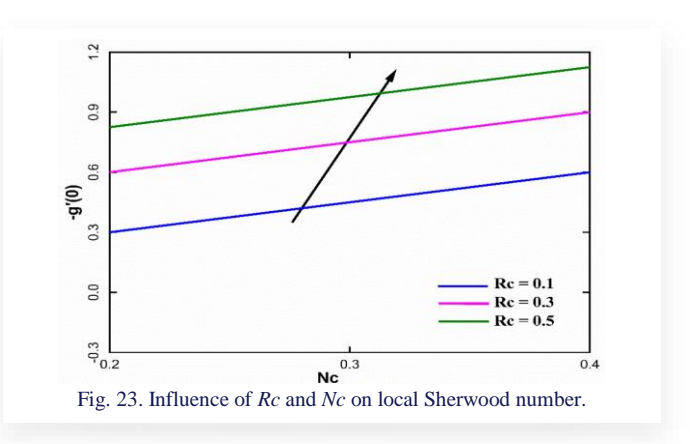


Fig. 22. Influence of Rc and Nbt on local Sherwood number.



The heat transfer rate, represented by the local Nusselt number, is influenced by several factors. Higher values of the thermophoresis parameter, power-law index (*n*), and conversely, increasing the convective parameter enhances the local Nu, suggesting improved heat transfer.

Notably, the power-law index (n), which describes the fluid's flow behaviour, has a consistently negative impact on the local Nu at the surface, meaning a more shear-thinning fluid will exhibit reduced heat transfer.

5. Conclusions

The numerical values for the parameters in this study were selected within realistic ranges observed in relevant engineering applications, such as microelectronics cooling, heat exchangers, and geothermal systems. For example, the Weissenberg number (We), which characterizes the fluid's elasticity, was varied to represent both Newtonian and viscoelastic behaviours, enabling a comprehensive investigation of how fluid elasticity influences the flow. A range of values was explored for each parameter to thoroughly analyse its impact on flow and heat transfer, providing a detailed understanding of their effects on velocity, temperature and concentration profiles. Furthermore, the chosen values were benchmarked against those used in previous studies on similar nanofluid, non-Newtonian and MHD flow problems, allowing for direct comparison and validation of the present results with existing literature.

In this investigation, the non-dimensional parameter values n = 0.5, We = 0.5, M = 2, Da = 0.5, Gr = 5, Gc = 5, Pr = 0.72, R = 0.5, Nc = 0.5, Le = 3, Nbt = 5, Q = 0.5, Ec = 0.5, Sc = 0.5, Rc = 10 were used. These variables are treated as constants except for changed parameters in the graphs. Boundary layer flow and heat transfer of HTF fluid with nanosized particles via a stretched sheet are often described in relation to thermal radiation, convective heating, Weissenberg number and magnetic field metric. Through the application of similarity transformation, the boundary layer equations controlling the flow issue are reduced to a pair of high order non-linear ODEs.

Using MATLAB's bvp4c, the resultant ODEs are numerically solved.

The fundamental results of the investigation are:

1. Increasing the Weissenberg number We or power-law index *n* thins the velocity boundary layer.

- 2. Radiation, however, increases the thickness of the thermal boundary layer.
- 3. Velocity, temperature and concentration fields for the flow of tangent hyperbolic fluid decline with the chemical reaction parameter.
- 4. The fluid velocity and temperature increase and the concentration profile drops with the increasing values of heat source/sink parameter.
- 5. The energy field is enhanced with the intensifying effect of porous parameter, but the velocity curve of HTF decreases.
- 6. Similarly, the skin friction coefficient C_f decreases as the slip parameter increases.
- 7. An increase in the Weissenberg number acts to reduce the skin friction coefficient.
- 8. Furthermore, the Weissenberg number has a diminishing effect on the local Nusselt number.
- 9. The convective metric and power-law index demonstrate opposite effects on the local Nusselt number.

References

- [1] Shankar Goud, B., Pramod Kumar, P., & Malga, B.S. (2022). Induced magnetic field effect on MHD free convection flow in non-conducting and conducting vertical microchannel walls. *Heat transfer*, 51(2), 2201–2218. doi: 10.1002/htj.22396
- [2] Al Oweidi, K.F., Jamshed, W., Goud, B.S., Ullah, I., Usman, Mohamed Isa, S.S.P., El Din, S.M., Guedri, K., & Jaleel, R.A. (2022). Partial differential equations modeling of thermal transportation in Casson nanofluid flow with Arrhenius activation energy and irreversibility processes. *Scientific Reports*, 12(1), 20597. doi: 10.1038/s41598-022-25010-x
- [3] Jamshed, W., Ramesh, G.K., Roopa, G.S., Nisar, K.S., Safdar, R., Madhukesh, J.K., Shahzad, F., Isa, S.S.P.M., Shankar Goud, B., & Eid, M.R. (2022). Electromagnetic radiation and convective slippery stipulation influence in viscous second grade nanofluid through penetrable material. ZAMM-Journal of Applied Mathematics and Mechanics (Zeitschrift für Angewandte Mathematik und Mechanik), e202200002. doi: 10.1002/zamm.202200002
- [4] Pal, D. (2009). Heat and mass transfer in stagnation-point flow towards a stretching surface in the presence of buoyancy force. *Meccanica*, 44(2), 145–158. doi: 10.1007/s11012-008-9155-1
- [5] Asogwa, K.K., Kumar, K.T., Goud, B.S., & Chohan, J.S. (2023). Significance of nanoparticle shape factor and buoyancy effects on a parabolic motion of EMHD convective nanofluid past a Riga plate with ramped wall temperature. *The European Physical Journal Plus*, 138(6), 1–13. doi: 10.1140/epjp/s13360-023-04170-3
- [6] Kandasamy, R., Muhaimin, I., & Saim, H.B. (2010). Lie group analysis for the effect of temperature-dependent fluid viscosity with thermophoresis and chemical reaction on MHD free convective heat and mass transfer over a porous stretching surface in the presence of heat source/sink. *Communications in Nonlinear Sci*ence and Numerical Simulation, 15(8), 2109–2123. doi: 10.1016/ j.cnsns.2009.09.016
- [7] Dharmaiah, G., Goud, B.S., Shah, N.A., & Faisal, M. (2023). Numerical analysis of heat and mass transfer with viscous dissipation, Joule dissipation, and activation energy. *International Journal of Ambient Energy*, 44(1), 2090–2102. doi: 10.1080/01430750.2023.2224335
- [8] Shankar Goud, B., & Dharmaiah, G. (2023). Role of Joule heating and activation energy on MHD heat and mass transfer flow in the presence of thermal radiation. *Numerical Heat Transfer, Part*

- B: Fundamentals, 84(5), 620–641. doi: 10.1080/10407790.2023. 2215917
- [9] Elbashbeshy, E.M.A., & Bazid, M.A.A. (2004). Heat transfer over an unsteady stretching surface. *Heat Mass Transfer*, 41, 1– 4. doi: 10.1007/s00231-004-0520-x
- [10] Raptis, A. (1998). Radiation and Free Convection Flow through a Porous Medium. *International Communications in Heat and Mass Transfer*, 25(2), 289–295. doi: 10.1016/S0735-1933(98) 00016-5
- [11] Cortell, R. (2007). Viscous flow and heat transfer over a nonlinearly stretching sheet. *Applied Mathematics and Computation*, 184(2), 864–873. doi: 10.1016/j.amc.2006.06.077
- [12] Xuan, Y., & Li, Q. (2000). Heat transfer enhancement of nanofuids. *International Journal of Heat and Fluid Flow*, 21(1), 58–64. doi: 10.1016/S0142-727X(99)00067-3
- [13] Malik, M.Y., Salahuddin, T., Hussain, A., & Bilal, S. (2015). MHD flow of tangent hyperbolic fluid over a stretching cylinder: Using Keller box method. *Journal of Magnetism and Magnetic Materials*, 395, 271–276. doi: 10.1016/j.jmmm.2015.07.097
- [14] Naseer, M., Malik, M.Y., Nadeem, S., & Rehman, A. (2014). The boundary layer flow of hyperbolic tangent fluid over a vertical exponentially stretching cylinder. *Alexandria Engineering Journal*, 53(3), 747–750. doi: 10.1016/j.aej.2014.05.001
- [15] Hayat, T., Qayyum, S., Ahmad, B., & Waqas, M. (2016). Radiative flow of a tangent hyperbolic fluid with convective conditions and chemical reaction. *European Physical Journal Plus*, 131(12). doi: 10.1140/epjp/i2016-16422-x
- [16] Nadeem, S., & Akram, S. (2009). Peristaltic Transport of a Hyperbolic Tangent Fluid Model in an Asymmetric Channel. *Zeitschrift für Naturforschung A*, 64(9–10), 559–567. doi: 10.1515/zna-2009-9-1004
- [17] Reddy, B.N., Dodda, R., & Reddy, B.S. (2024). A Numerical Investigation on Boundary Layer Flow of MHD Tangent Hyperbolic Fluid Flow over a Stretching Sheet with Slip Boundary Conditions. *Journal of Advanced Research in Fluid Mechanics and Thermal Sciences*, 120(1), 122–139. doi:10.37934/arfmts. 120.1.122139
- [18] Upadhya, S.M., Raju, S.S.K., Raju, C.S.K., & Mnasri, C. (2020). Arrhenius Activation and Zero Mass Flux Conditions on Nonlinear Convective Jeffrey Fluid over an Electrically Conducting and Radiated Sheet. *Arabian Journal for Science and Engineering*, 45(11), 9095–9109. doi: 10.1007/s13369-020-04687-0
- [19] Nadeem, S., & Akram, S. (2011). Magnetohydrodynamic peristaltic flow of a hyperbolic tangent fluid in a vertical asymmetric channel with heat transfer. *Acta Mechanica Sinica*, 27(2), 237–250. doi: 10.1007/s10409-011-0423-2
- [20] Sheikh, M., Hasnain, J., Abid, N., & Abbas, Z. (2024). Chemically reactive mhd flow through a slendering stretching sheet subjected to non-linear radiation flow over a linear and non-linear stretching sheet. *Facta Universitatis, Series: Mathematics and Informatics*, 39(2), 265–278. doi: 10.22190/fumi230413018s
- [21] Nasir, S., Berrouk, A.S., & Aamir, A. (2024). Efficiency analysis of solar radiation on chemical radioactive nanofluid flow over a porous surface with magnetic field. *Case Studies in Thermal En*gineering, 63, 105231. doi: 10.1016/j.csite.2024.105231
- [22] Gaffar, S.A., Bég, O.A., Kuharat, S., & Bég, T.A. (2024). Computation of hydromagnetic tangent hyperbolic non-Newtonian flow from a rotating non-isothermal cone to a non-Darcy porous medium with thermal radiative flux. *Physics Open*, 19, 100216. doi: 10.1016/j.physo.2024.100216
- [23] Shehzad, S.A., Hayat, T., Qasim, M., & Asghar, S. (2013). Effects of mass transfer on MHD flow of Casson fluid with chemical reaction and suction. *Brazilian Journal of Chemical Engineering*, 30(1), 187–195. doi:10.1590/S0104-66322013000100020

- [24] Amjad, M., Khan, M.N., Ahmed, K., Ahmed, I., Akbar, T., & Eldin, S.M. (2023). Magnetohydrodynamics tangent hyperbolic nanofluid flow over an exponentially stretching sheet: Numerical investigation. *Case Studies in Thermal Engineering*, 45, 102900. doi: 10.1016/j.csite.2023.102900
- [25] Ahmed, I., Alghamdi, M., Amjad, M., Aziz, F., Akbar, T., & Muhammad, T. (2023). Numerical investigation of MHD flow of hyperbolic tangent nanofluid over a non-linear stretching sheet. *Helion*, 9(7), e17658. doi: 10.1016/j.heliyon.2023.e17658
- [26] LeVeque, R.J. (2007). Finite difference methods for ordinary and partial differential equations. Steady-state and time-dependent problems. Society for Industrial and Applied Mathematics. Philadelphia, USA.